Nuclear Engineering and Technology 51 (2019) 1047–1059

Contents lists available at ScienceDirect

Nuclear Engineering and Technology

journal homepage: www.elsevier.com/locate/net

Original Article

Development of a multiphysics numerical solver for modeling the behavior of clay-based engineered barriers

Vicente Navarro [a, *], Laura Asensio [a], Heidar Gharbieh [b], Gema De la Morena [a], Veli-Matti Pulkkanen [b]

[a] Geoenvironmental Group, University of Castilla-La Mancha, Avda. Camilo José Cela s/n, 13071, Ciudad Real, Spain
[b] VTT Technical Research Centre of Finland Ltd, Espoo, Finland

ARTICLE INFO

Article history:
Received 14 November 2018
Received in revised form
16 January 2019
Accepted 7 February 2019
Available online 10 February 2019

Keywords:
Deep geological repository
Clay-based barrier
Compacted bentonite
Multiphysics modeling
Thermo-hydro-chemo-mechanical behavior

ABSTRACT

This work describes the development of a numerical module with a multiphysics structure to simulate the thermo-hydro-chemo-mechanical behavior of compacted bentonites. First, the conceptual model, based on the state-of-the-art formulation for clay-based engineered barriers in deep geological repositories, is described. Second, the advantages of multiphysics-based modules are highlighted. Then, the guidelines to develop a code using such tools are outlined, presenting an example of implementation. Finally, the simulation of three tests that illustrate the behavior of compacted bentonites assesses the scope of the developed code. The satisfactory results obtained, and the relative simplicity of implementation, show the opportunity of the modeling strategy proposed.

1. Introduction

The safe disposal of high level radioactive waste is an environmental issue of the utmost importance, key in the integral and responsible conception of nuclear fission technology for energy supply [1]. Among the different strategies considered, the most established is the disposal in deep geological repositories, whose design includes natural barriers and engineered barrier systems (EBS) to isolate the radioactive particles from the biosphere [2]. Clay-based barriers, made of compacted bentonite, will be a part of the EBS in different repository concepts in crystalline and argillaceous host rock, often termed as buffer and/or backfill [3,4]. Since the safety of deep geological repositories for high level radioactive waste must be ensured for hundreds of thousands of years, numerical simulation is a useful strategy to obtain plausible estimations of the future behavior of the system.

The behavior of the bentonite barriers will be strongly influenced by the initial heterogeneities that may occur in the contact between the different components considered in their design (compacted blocks, foundation layers and pellets), or that may be caused by errors in the manufacture and/or installation of these components. For this reason, obtaining a reliable prediction of the evolution of the heterogeneities is essential for a consistent assessment of the repository functionality. Since homogeneity is dependent on the continuous distribution of density, and density defines the packing of the soil skeleton, changes in homogeneity are caused by the changes in the soil skeleton arrangement, that is, by the soil strains. Thus, the numerical model must be able to define the evolution of the spatial distribution of strains to characterize the evolution of homogeneity. Therefore, a mechanical (M) model that allows the estimation of displacements, and thus strains, must be adopted. The model must also be able to estimate the stress state to compute the confinement stress, or swelling pressure, which conditions the barrier functionality [5].

In bentonites like those to be used in EBS, the coupling between hydraulic and mechanical behavior is very strong. Then, an adequate characterization of the mechanical behavior of the system needs a coupled hydraulic (H) model. Given the important role that an increase in gas pressure (caused by the saturation of bentonite, or associated with the production of gas that could derive from processes such as the corrosion of the metal canister containing radioactive waste) can play in both the flow and the mechanical problem, the hydraulic model should be understood as an extended flow model that, together with water, includes the analysis of gas flow.

* Corresponding author.
E-mail address: vicente.navarro@uclm.es (V. Navarro).

https://doi.org/10.1016/j.net.2019.02.007

Besides, under low confinement conditions, such as those usually associated with initial heterogeneities, the swelling caused by the hydration of bentonite aggregates can play a significant role. It is therefore advisable to adopt a double porosity approach capable of modeling not only the change of the inter-aggregates porosity (macroporosity), but also the change of the intra-aggregate porosity (microporosity) due to hydration. Since this hydration process is conditioned by the salinity of the system [6], the model needs to include a geochemical formulation (c, for chemical), even if it is a simplified one (lowercase c), thus allowing to analyze the sensitivity of volumetric strains to salinity.

Last, all the described hydro (flow) -chemo-mechanical processes affect and are affected by temperature. For this reason, to characterize the temperature distribution (T problem), a coupled heat transfer analysis is needed.

In summary, a THMc conceptual and numerical model based on a double porosity framework should be used for the assessment of the complete performance of the system.

The broad experience in the application of HM and THM formulations for the characterization of the field behavior of EBS (see, for instance Refs. [7,8]), and the developments to solve problems including the effect of salinity (for instance Refs. [9,10]), provide the necessary background. They define the THMc conceptual model to be adopted, providing the set of equations to formalize this conceptual model in a mathematical object, formulated as a boundary value problem, whose resolution will allow describing the behavior of the system.

When conceiving a numerical tool to solve such boundary value problems, it is of interest to consider the evolution experienced recently by the Multiphysics Partial Differential Equations Solvers (MPDES). It is not straightforward to model complex geochemical systems with them. However, if a simplified geochemical model is assumed ("lowercase c"), as it is done in this paper, these solvers are flexible and versatile enough to couple or disable other physical problems under consideration, allowing the user to adapt the numerical tools to the conceptual approximation desired to treat each problem. Some programs, as, for instance, Comsol Multiphysics (CM) [11], use a symbolic algebra interface to treat the differential equations introduced by the user, and apply automatic symbolic differentiation techniques that improve the numerical performance (see, for instance Ref. [12]). In addition, the state functions used in the differential equations are introduced as text lines. Thus, the numerical implementation is not very different from using a notebook and requires little effort. Therefore, disregarding the modeling of localization processes (such as cracking or the development of preferential flow paths), the continuum MPDES offer an opportunity to obtain an efficient numerical tool to model the THMc behavior of clay-based EBS.

The aim of this work is to outline the guidelines to develop a tool of such kind. This way, numerical simulation techniques will be made more accessible for other research groups linked to the analysis of EBS, especially emerging groups, making it easier for them to contribute to the characterization of the behavior of clay-based EBS.

2. Conceptual model

2.1. System abstraction

Based on the bimodal distribution of porosity observed using porosimetry techniques [13] (see Fig. 1a), a double porosity approach is proposed to model the compacted bentonites behavior

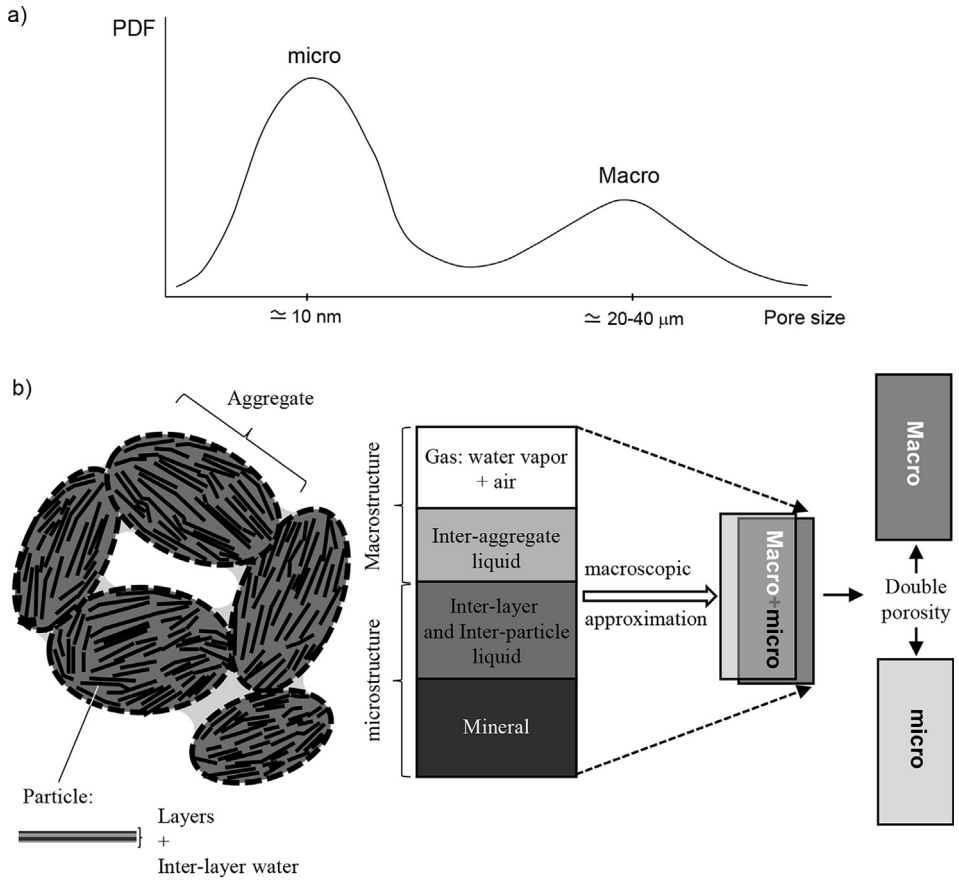

Fig. 1. (a) Typical pore size distribution result of a mercury intrusion porosimetry (PDF, Pore Distribution Frequency). (b) Idealization of soil phases.

(see, for instance Refs. [9,14]). As noted, in this approach, the macrostructure is associated with the space between bentonite particle aggregates, while the microstructure (which is usually assumed to be saturated [14,15]) is associated with their internal voids. Each structural level is assigned to a different continuum medium, while both media occupy the same spatial domain [16] (Fig. 1b).

The mass exchange between the two structural levels can be interpreted as a phase change process governed by the difference between chemical potentials [17]. Based on this idea, Navarro et al. [17,18] proposed a non-linear formulation that obtained good results when modeling free swelling processes in MX-80 bentonite [10]. This is the mass exchange formulation adopted in this paper. The approach uses the adsorbed water density, ρ_m. However, although some authors have noted that ρ_m may be greater than the density of free water ρ_W (see Ref. [19], for instance), $\rho_m = \rho_W$ is assumed for modeling purposes [20].

Both macrostructural and microstructural water can have dissolved chemical species. Since the salinity will condition the soil's deformational behavior [21], geochemical couplings are needed in the model. An idealized geochemical configuration is proposed, which simplifies the system, in addition to the clay mineral, to two cations (for instance, Na^+ and Ca^{2+}) and only one anion (generally, Cl^-). Although this kind of models have limitations to reproduce realistic conditions [22], they obtain satisfactory results in the simulation of complex processes such as the free swelling of MX-80 bentonite subject to relevant salinity changes [10,23]. Consequently, even if their simulation capacity is limited, they are valid tools to evaluate the sensitivity of the system to salinity changes.

The Donnan equilibrium approach [20,24] is proposed to be applied, see Table 1. Hence, dissolved ions in the macrostructure are assumed to be in equilibrium with those in the microstructure, introducing the effect of the charged clay particles (that is, their cationic exchange capacity) through the Donnan potential, an electrostatic potential that is assumed zero (reference value) in the macrostructure. Anion exclusion is not imposed [20]. Therefore, Cl^- may be present in the microstructure, and its distribution between macrostructure and microstructure is only conditioned by the electrochemical equilibrium, determined from the equality of electrochemical potentials. Analogously, the distribution of Na^+ and Ca^{2+} between both structural levels will also be determined from the equality of electrochemical potentials, and thus it will condition cationic exchange.

In addition, electroneutrality is assumed in the macrostructure and the microstructure (Table 1). This leads to three chemical equilibrium equations (equilibrium between macrostructural and microstructural Na^+, Ca^{2+} and Cl^-) and two electroneutrality equations. Among the seven variables defining the salinity in this system (six concentrations of three ions in macrostructure and microstructure, and the Donnan potential), it is possible to select two degrees of freedom. The formulation is simplified if, as proposed by Navarro et al. [10], the macrostructural Ca^{2+} concentration and the microstructural Cl^- concentration are selected as state variables to characterize salinity.

To formulate a conceptual model as simple as possible, gas is assumed to consist only of water vapor and "dry" air, or simply air (see Fig. 1b), both considered to be perfect gases. Since the microstructure is assumed saturated, gas will only be present in the macrostructural voids. As noted in Posiva [25], a large part of the gas flow can occur through a network of pathways induced by the gas pressure. The simulation of the development of these flow paths (that is, the aperture or "break-through", and sealing or "shut-in") is complex. For this reason, as stated in the Introduction, the simulation of the gas flow is considered only in a continuum, with a variable homogeneity, but where the existence of potential preferential flow paths would require the explicit definition of the path geometry. To include the possible development of preferential flow paths along existing or pressure-dependent discontinuities the work by Olivella and Alonso [26] should be of interest.

Given the existing strong thermo-mechanical and thermo-hydraulic couplings, heat transfer should be introduced in the model. For this purpose, there are three primary mechanisms to be considered: convection, conduction and radiation. Radiation is generally neglected with respect to conduction [27]. Although in some cases convection is also neglected with respect to conduction [27,28], it is advisable to take this term into account to correctly simulate the partially saturated behavior of the system.

Finally, local thermal equilibrium is assumed between the soil constituents [8,29]. This means that, although the value of temperature can be different at each point of the domain, all the phases and species are at the same temperature in a determined point. Hence, only one heat transfer equation is needed.

2.2. State variables, balance and field equations, and state functions

Following the system abstraction proposed in the previous section, the soil conditions are defined by seven state variables: $\mathbf{u}$, vector of the solid skeleton displacements; e_m, microstructural void ratio (volume of intra-aggregate voids per volume of the mineral), which defines the packing of the microstructure; P_L, macrostructural liquid pressure; P_G, gas pressure; C_{CaM}, molar calcium concentration in the macrostructure; C_{Clm}, molar chloride concentration in the microstructure; and T, temperature. To compute their values, six balance equations (whose associated state variables are in Table 2) and the mechanical equilibrium equation (which will determine $\mathbf{u}$) must be solved.

2.2.1. Balance equations. Flow, transport and heat transfer model

All balance equations follow the same structure (see, for instance Refs. [8,29]):

$$\frac{\partial m_*}{\partial t} + \nabla \cdot \mathbf{l}_* = r_* \tag{1}$$

where the expressions "$\partial(\ )/\partial t$" and "$\nabla\cdot(\ )$" define the partial time derivative and the divergence operator, respectively; m_* is the volumetric density of the magnitude balanced (see Table 3), and r_* represents a mass source term. This term is null except when

Table 1
Equations used to model the salinity condition. $C_{i,M}$ and $C_{i,m}$ ("i": Cl^-, Na^+, and Ca^{2+}) are the molar concentrations in both structural levels, Ψ_D is the Donnan potential, *CEC* is the cationic exchange capacity, $\rho_{mineral}$ is the mineral density, and e_m is the microstructural void ratio (see Section 2.2).

Donnan equilibrium (adapted from Ref. [20])	$C_{i,M} = C_{i,m} \cdot \exp\left(\frac{z_i \cdot F \cdot \Psi_D}{R \cdot T}\right)$
Macrostructural electroneutrality	$C_{Na,M} + 2 \cdot C_{Ca,M} - C_{Cl,M} = 0$
microstructural electroneutrality	$C_{Na,m} + 2 \cdot C_{Ca,m} - C_{Cl,m} - q = 0$
Surface charge (eq/L)	$q = \frac{CEC \cdot \rho_{mineral}}{e_m}$

Table 2
Problem ID: balance equation and associated state variable.

ID	Balance	State variable
1	Macrostructural water mass	Macrostructural liquid pressure, P_L
2	Microstructural water mass	Microstructural void ratio, e_m
3	Air mass	Gas pressure, P_G
4	Total Ca^{2+} mass	Macrostructural molar concentration of Ca^{2+}, C_{CaM}
5	Total Cl^- mass	Microstructural molar concentration of Cl^-, C_{Clm}
6	Enthalpy	Absolute temperature, T

balancing macrostructural water mass, where $r_W = -\rho_W\, c_m$ (c_m is the macrostructural water volume moving to the microstructure per soil unit volume; see Ref. [18]), and microstructural water mass, where $r_m = \rho_W\, c_m$. Vector $\mathbf{l}_*$ defines the flow associated with each balance equation (Table 3). In the five first cases in Table 3, it is a mass flow per unit surface area per time. In the last case, it is an energy flow. These flows are given by the solid skeleton velocity vector $\mathbf{v}$ (time derivative of $\mathbf{u}$), and the field equations in Table 4. The macrostructural liquid water specific discharge $\mathbf{q}_{ML}$ is computed using the advective formulation proposed by Pollock [30], although different state functions are proposed to be used. Hence, the macrostructural degree of saturation for water Sr_M (function of the macrostructural suction s_M, identified as the capillary suction, and therefore calculated as the difference between gas and liquid pressures) is proposed to be calculated using a van Genuchten [31] retention curve, but applying the approach of Navarro et al. [18] to obtain differentiated models of the intra-aggregate (microstructural) and inter-aggregate (macrostructural) water content. The macrostructural liquid relative permeability κ_{ML} can be modeled using the Brooks and Corey [32] formulation, assuming an exponent value of 3 for the macrostructural degree of saturation for water [7]. The macrostructural liquid intrinsic permeability k_{ML} is assumed to be isotropic and the model proposed by Gens et al. [7] is applied. All these functions are presented in Table A1 (Appendix A), which includes all the state functions involved in the flow model.

Like the macrostructural liquid water specific discharge, the advective gas flow $\mathbf{q}_G$ is proposed to be modeled with a generalized Darcy's law [33]. Given the small value of gas density, the gas pressure gradient ∇P_G can be taken as driving force, neglecting the gravitational term ($g\ \nabla z$, where g is the gravitational acceleration and z is the vertical coordinate upward oriented) in the gas flow equation [34]. If the intrinsic permeability is assumed to be a soil property linked to its structure, the gas intrinsic permeability k_G should be equal to that of water. However, experimental issues [35], the slip flow (or Klinkenberg effect) and the presence of inertial effects [33] might cause the gas intrinsic permeability to be greater than that of macrostructural water. To take this into account, is it advisable to consider assigning different values to water and gas intrinsic permeabilities. This is the case in Table A1, where the expressions of the intrinsic and relative (κ_G) permeabilities derived from Yoshimi and Ostenberg [34] has been adopted for the gas.

Table 4
Field equations used to calculate flows $\mathbf{l}_*$ in Table 3.

ID		Equation
1, 4, 5, 6	$\mathbf{q}_{ML}$	$\mathbf{q}_{ML} = -\frac{k_{ML}k_{ML}}{\mu_{ML}}(\nabla P_L + \rho_W g\ \nabla z)$
1, 3, 6	$\mathbf{q}_G$	$\mathbf{q}_G = -\frac{k_G k_G}{\mu_G}\nabla P_G$
1, 3, 6	$\mathbf{i}_V$	$\mathbf{i}_V = -\tau_V\,\phi_M(1-Sr_M)\rho_G\, D_V \nabla\left(\frac{\rho_V}{\rho_G}\right)$
3, 6	$\mathbf{i}_A$	$\mathbf{i}_A = -\mathbf{i}_V$

The vapor flow is usually simulated using an advective/dispersive model [36]. The advective component is linked to the advective flow of the whole gas phase, described in the previous paragraph. Assuming that the magnitude of this flow is not high, the hydrodynamic dispersion term of diffusion can be disregarded, then identifying diffusion with molecular diffusion $\mathbf{i}_V$. The binary diffusion coefficient of water vapor in gas D_V can be calculated as proposed by Pollock [30] and Philip and De Vries [37], while the soil tortuosity to vapor flow τ_V can tentatively be assumed equal to 1, like Olivella and Gens [38] (see Pintado et al. [39] for information on how to identify higher quality τ_V values). To determine the density of water vapor ρ_V, the psychrometric law can be applied [40], using the formulation in Ewen and Thomas [41] to calculate the density of saturated water vapor ρ_{VO} (Table A1).

As gas is assumed to consist of only two components, the sum of their diffusion terms must be zero [29]. Consequently, the diffusion of air $\mathbf{i}_A$ is a vector of the same magnitude of $\mathbf{i}_V$ and opposite direction.

There is an additional advective term in the modeling of air flow, the one corresponding to the air dissolved in the macrostructural

Table 3
Volumetric density and flow terms associated with the balance equations in Table 2.

ID	m_*	$\mathbf{l}_*$
1	$m_W = m_{ML} + m_V = = \rho_W\frac{e_M\ Sr_M}{1+e} + \rho_V\frac{e_M(1-Sr_M)}{1+e}$	$\mathbf{l}_W = m_W\mathbf{v} + (\rho_W\mathbf{q}_{ML}) + (\rho_V\mathbf{q}_G + \mathbf{i}_V)$
2	$m_m = \rho_W\frac{e_M}{1+e}$	$\mathbf{l}_m = m_m\mathbf{v}$
3	$m_A = \rho_A\frac{e_M(1+Sr_M(1-H))}{1+e}$	$\mathbf{l}_A = m_A\mathbf{v} + \rho_A\mathbf{q}_G + \mathbf{i}_A + \rho_A H\ \mathbf{q}_{ML}$
4	$m_{Ca} = \frac{C_{CaM}\ Sr_M\ e_M + C_{Cam}\ e_m}{1+e}$	$\mathbf{l}_{Ca} = m_{Ca}\mathbf{v} + C_{CaM}\mathbf{q}_{ML} - D_{CaM}\nabla C_{CaM} - -D_{Cam}\nabla C_{Cam}$
5	$m_{Cl} = \frac{C_{ClM}\ Sr_M\ e_M + C_{Clm}\ e_m}{1+e}$	$\mathbf{l}_{Cl} = m_{Cl}\mathbf{v} + C_{ClM}\mathbf{q}_{ML} - D_{ClM}\nabla C_{ClM} - -D_{Clm}\nabla C_{Clm}$
6	$h = \frac{\rho_{mineral}h_{mineral}}{1+e} + m_{ML}h_{ML} + m_V h_V + +m_m h_m + m_A h_A$	$\mathbf{l}_h = h\ \mathbf{v} + \rho_W h_{ML}\mathbf{q}_{ML} + h_V(\rho_V\mathbf{q}_G + \mathbf{i}_V) + +h_A(\rho_A\mathbf{q}_G + \mathbf{i}_A + \rho_A H\ \mathbf{q}_{ML}) - -\lambda\nabla T$

water (Table 3). The amount of dissolved air in the macrostructural water is calculated using Henry's constant H or volumetric coefficient of solubility of air in water [29]. This dimensionless coefficient is in fact a function that changes with temperature [42] (see Table A1).

As usual in transport formulations (see for instance Ref. [43]), the total mass flow of Ca^{2+} and Cl^{-} is computed as the sum of advective flow plus the dispersive flow. The advective mass flow is calculated as the product of the macrostructural liquid water specific discharge by the macrostructural concentration of the ions. Because the modulus of this flow is usually small, mechanical dispersion is neglected, and the total diffusion is assumed to be equal to the molecular diffusion, modeled using Fick's law, see Table 4. The formulation by Bourg et al. [44] is proposed to determine the molecular diffusion coefficients D_{i^*} (i = Ca or Cl), both in the macrostructure (* = M) and the microstructure (* = m). The values used by Cussler [45] can be taken as a first approximation of the self-diffusion coefficients, D_{Oi} (i = Ca or Cl).

Fourier's law is used to define the conductive flow of enthalpy (variable used in this work to define the balance and flow of energy, see Table 3). The thermal conductivity λ is assumed, like the intrinsic permeability, to be isotropic. As a first option, λ can be computed as the volume-weighted average of the thermal conductivity of dry soil, macrostructural water, water vapor and air [29]. However, it could be of interest to assess the application of different formulations, such as those used by Sánchez et al. [8] and Pollock [30], which are based on averaging the conductivities of dry and saturated soil. The advective flow of enthalpy can be calculated as the sum of the products of the specific enthalpies of macrostructural water (h_{ML}), vapor (h_V) and air (h_A) by their respective volumetric flows (Table 3). These specific enthalpies, and those of the soil mineral and microstructural water (both necessary for the energy balance, see Table 3), can be computed using the linear laws proposed by Pollock [30]. This reference also provides the value of the latent heat of vapor, which plays a very important role in heat transfer.

As illustrated in Sections 5.1 and 5.2, if a multiphysics numerical solver is used to implement the numerical model, it is fairly easy to modify any of the state functions involved in any field equation. In consequence, the functions previously described, as well as any of those described in the document, can be modified if desired.

2.2.2. Mechanical model

In the model, mechanical equilibrium is met by applying the Principle of Virtual Works, which is the weak form of the mechanical equilibrium equation:

$$\nabla\cdot\boldsymbol{\sigma} - \rho\ g\ \nabla z = \mathbf{0} \tag{2}$$

where $\boldsymbol{\sigma}$ is the total stress vector (the engineering or Voigt notation is used for both stress and strain tensors), and ρ is the bulk soil density. Although $\boldsymbol{\sigma}$ defines the equilibrium, it does not determine the deformability of the soil. Focusing on the macrostructure, if it is assumed that the volume of the microstructure remains constant, it is usual to consider that the macro-strains $d\boldsymbol{\varepsilon}_M$ are caused by the changes of two "significant stresses", the macrostructural matric suction s_M and the net stress $\boldsymbol{\sigma}'' = \boldsymbol{\sigma} - P_G\cdot\mathbf{m}$ (where $\mathbf{m}$ is the vector form of the Kronecker delta), and by the changes of T. However, in general, the volume of the microstructure will change, and the increase of total strain $d\boldsymbol{\varepsilon}$ is computed using an additive formulation:

$$d\boldsymbol{\varepsilon} = d\boldsymbol{\varepsilon}_m + d\boldsymbol{\varepsilon}_{Mm} + d\boldsymbol{\varepsilon}_M \tag{3}$$

where $d\boldsymbol{\varepsilon}_m$ is the increase of microstructural strain caused by the change in volume of aggregates, and $d\boldsymbol{\varepsilon}_{Mm}$ defines the rearrangement of the macrostructure as a consequence of $d\boldsymbol{\varepsilon}_m$. It is accepted that the rearrangement of the macrostructure does not affect the arrangement of the microstructure [46].

Under isothermal conditions, the critical state model presented by Alonso et al. [47], known as Barcelona Basic Model or BBM, is proposed to compute $d\boldsymbol{\varepsilon}_M$. The model, formulated in terms of two significant stresses, net stress and macrostructural suction, has become the reference model in unsaturated soil modeling. Most of the researchers working within unsaturated soil mechanics use the BBM or formulations derived from it, or structure their models having the BBM as a reference (see the reviews by Refs. [48,49], for instance).

The thermo-mechanical coupling in the macrostructural strain behavior can be introduced using an elastic model like that of Ma and Hueckel [50]. The nonlinear law by Sánchez et al. [8] can be used to compute the macrostructural bulk modulus for changes in temperature.

If $d\boldsymbol{\varepsilon}_m$ is assumed isotropic its value is given by the variation of e_m. To calculate this variation, the definition of the microstructural void ratio given in Fig. 2 (based on the analysis of the change of the microstructural water content, or microstructural void ratio, for a wide number of MX-80 samples [18]) is taken into account. In the figure, π defines the thermodynamic swelling pressure [51], and e_{mR} is the remaining microstructural void ratio under dry conditions.

The tensor $d\boldsymbol{\varepsilon}_{Mm}$ is also proposed to be assumed isotropic. Then, its volumetric value $d\varepsilon^V_{Mm}$ will be enough to characterize it. According to Navarro et al. [10], two components can be distinguished in the coupling between macrostructural and microstructural strains. The first, $d\varepsilon^V_{Mm1}$, occurs because of changes in the macrostructural packing. It can be computed as proposed by Alonso et al. [56] when adapting the BBM to reproduce the behavior of double porosity expansive soils, giving rise to the Barcelona Expansive Model (BExM). The second component, $d\varepsilon^V_{Mm2}$, describes the free swelling caused in the macrostructure (generation of macrostructural void ratio e_M, defined as the volume of inter-aggregate voids per volume of the mineral) by the microstructure destructuration under conditions of low confinement. Under such conditions, the breaking up of clay particles and aggregates into smaller units generates new void space [57]. This magnitude is proposed to be computed using the formulation presented Navarro et al. [10], which, as illustrated in Section 5.3, obtains satisfactory fits when simulating free swelling processes under variable salinity

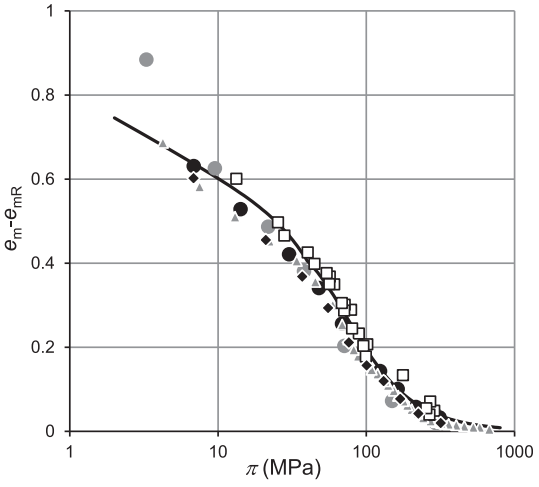

Fig. 2. Microstructural void ratio e_m as a function of the thermodynamic swelling pressure π. Symbols: data from Dueck and Nilsson [52] (grey and black dots), Kahr et al. [53] (triangles), Sane et al. [54] (squares), Wadsö et al. [55] (diamonds).

conditions.

3. Numerical model. Use of a multiphysics implementation environment

The group of equations defined in the previous section defines a nonlinear system of coupled partial differential equations, to be solved applying numerical techniques. Given the multiphysics nature of the problem, the use of a MPDES is highly recommended. As indicated in the Introduction, with tools of this kind, the user can focus on the definition of the governing balance equations and constitutive formulation, and the software takes automatic control of assembling the system of equations and solving it.

In addition, the physical processes included in the resolution of the problem can be adapted to the desired model. With no additional implementation effort, any of the balance equations can be decided not to be considered. In the resulting numerical problem, the corresponding state variables (Table 2) will not be solved for. The variables will still be defined and will remain constant at their initial value. Therefore, the numerical model can be simplified to match the desired conceptual model. In the same way, the model can be made more complex by adding new physical processes that, if solved, are automatically coupled to the rest. Then, in the future, the geochemistry of the soil, for instance, could be characterized in more detail by introducing new chemical species into the model. Both are capacities of interest. The first makes it easy to analyze the sensitivity of a problem to the consideration of different magnitudes (e.g., gas pressure gradients, temperature gradients). The second allows the code to evolve whenever more physical processes are deemed necessary to improve the conceptual model of the system.

Among the existing MPDES, CM [11] is considered a very convenient option for the coupled problems discussed. As mentioned in the Introduction, this software, based on the application of the finite element method with Lagrange multipliers, applies automatic symbolic differentiation techniques [12] to obtain the derivatives needed to define the iteration matrix. This significantly improves the computational convergence rate [58]. However, the use of a symbolic iteration matrix may cause problems when the formulation includes a state function that is defined implicitly. In this case, the chain rule cannot be applied, the program cannot define the derivatives involving that state function, and the calculation process cannot be started. That would be the case of implementing an elastoplastic formulation, as that previously described, or a non-linear state surface, as that used in the exercise in Section 5.2. Navarro et al. [59] proposed the use of a mixed method to avoid this problem, introducing the stresses and plastic variables as new state variables. Efficient and accurate solutions were obtained using this method [10,59,60], without finding the stability problems described in some cases of application of mixed methods [61].

CM includes different strategies of spatial discretization of the differential equations considered. In particular, discontinuous Galerkin methods can be used to reduce the problems with local mass balance conservation that are sometimes associated with the finite element method. To improve the simulation of front propagation, the program includes adaptive mesh refinement [11]. Likewise, finite strains associated with swelling problems can be simulated using Arbitrary Lagrangian-Eulerian techniques with remeshing [11]. Furthermore, given the versatility of the programming platform offered by CM, the user can implement a Lagrangian formulation of the problem [62]. To end this section, it should be noted that the finite element mesh definition capabilities in CM, as well as the remeshing option itself, can help to solve numerical oscillation problems associated with the advective flow.

4. Guidelines for implementing a multiphysics numerical solver

To implement the conceptual model described in Section 2, the seven tasks defined in Fig. 3 must be completed. The first task is to create a library that includes all those variables with a defined functional dependence (generically, “dependent variables”, DV), and related to the balance equations. This library, identified as “B-L” (balance library), contains the field equations in Table 4, the state functions in Table 3 and the variables linked to these functions. As indicated in the Introduction, in some MPDES, like CM, symbolic algebra allows to introduce these functions in text form, and the B-L can be simply imported from a text file. The part of the B-L corresponding to flow would consist of the text in Table A1 (after pertinently writing algebraic operations), which contains the flow DV as an example. Consulting the references in Section 3, the DV corresponding to transport and heat transfer can be written analogously. This way, the B-L would be complete.

Note that not all DV are used in all problems. For instance, if only isothermal problems are to be solved, the B-L does not need to include those DV related only with equation (or “problem ID”) number 6 (enthalpy balance) in Table 2.

The second task (Fig. 3) is to develop a “mechanical library” (M-L), which includes the functions needed to define the increment of net stress $d\boldsymbol{\sigma}''$, and $dp_O{}^*$, increment of the saturated preconsolidation stress $p_O{}^*$, plastic parameter of the BBM. The computation of these increments depends on the value of both variables [59]. As stated above, to avoid problems with the automatic symbolic differentiation, it can be assumed that $\boldsymbol{\sigma}''$ and $p_O{}^*$ are state variables (or “main unknowns”, MUs). To this end, two new equations must be defined, in which the new MUs are the variables solved for. Unlike the rest of MUs ($\mathbf{u}$, e_m, P_L, P_G, C_{CaM}, C_{Clm}, and T which are computed with partial differential equations, PDEs: Eqs. (1) and (2)), these are proposed to be computed with an ordinary differential equation (ODE) each. In the first, the time derivative of $\boldsymbol{\sigma}''$ will be set as the value of $d\boldsymbol{\sigma}''$ defined in the M-L. In the second, analogously, the time derivative of $p_O{}^*$ will be set as the value of $dp_O{}^*$ in the M-L. In CM, it is possible to define these equations as ODEs. In other solvers that do not have this option, they can be substituted by PDEs in which the flow term is made identically null [59]. The updating of $\boldsymbol{\sigma}''$ and $p_O{}^*$ using the values of $d\boldsymbol{\sigma}''$ and $dp_O{}^*$ defined in the M-L is the third task in the development of the numerical model (Fig. 3).

The value of $\boldsymbol{\sigma}''$ obtained after task 3 must meet a consistency criterion. When used together with P_G (or P_L in a saturated case) to

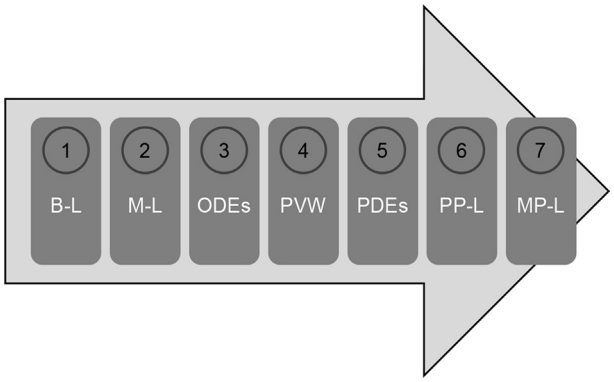

Fig. 3. Tasks to be performed to develop a THMc numerical model in a multiphysics programming environment that uses symbolic algebra-based calculations.

calculate $\boldsymbol{\sigma}$, the total stress computed must be statically admissible. This is, in combination with the estimation of the total strain obtained from $\mathbf{u}$ must meet the Principle of Virtual Works in a weighted way. Checking that this consistency criterion is met is the fourth task in the implementation of the model (Fig. 3).

The fifth task is introducing the PDEs in Table 2 into the MPDES (Fig. 3). Usually, MPDES offer an interface to introduce PDEs that presents a certain structure. If that structure meets the structure of Eq. (1), the implementation is simple, given that m_* (m_W, m_m, m_A, m_{Ca}, m_{Cl}, h), $\mathbf{l}_*$ ($\mathbf{l}_W$, $\mathbf{l}_m$, $\mathbf{l}_A$, $\mathbf{l}_{Ca}$, $\mathbf{l}_{Cl}$, $\mathbf{l}_h$) and r (r_W and r_m) are defined in the B-L. In that case, these terms only need to be indicated (referring to the library) in the interface equation editor. However, the structure can be different in other cases. For instance, the general structure of a PDE in CM is given by the following expression:

$$F_*\frac{\partial U_*}{\partial t} + \nabla\cdot\mathbf{l}_* = f_* \tag{4}$$

where U_* is the state variable for the analyzed physical process, $\mathbf{l}_*$ is defined in Eq. (1), and F_* and f_* are two functions to be defined. Adapting Eq. (1) to this structure is simple: the chain rule must be applied to obtain the time derivative of m_* as a function of the time derivatives of the MUs, and the definition of $\mathbf{l}_*$ in Tables 3 and 4 must be considered. As an example, for the mass of macrostructural water, $U_* = P_L$, and the following will hold:

$$F_W = \frac{\partial m_W}{\partial P_L};\quad f_W = r_W - \left(\sum_{U_*}\frac{\partial m_W}{\partial U_*}\frac{\partial U_*}{\partial t} + \nabla\cdot(m_W\mathbf{v})\right) \tag{5}$$

where, in this case, $U_* = \mathbf{u}$, e_m, P_G, C_{CaM}, C_{Clm}, and T. The partial derivatives, with respect to both the MUs and time, can be computed by the code thanks to its ability to make symbolic computations. The definition of F_W and f_W, and of F_m, f_m, F_A, f_A, F_{Ca}, f_{Ca}, F_{Cl}, f_{Cl}, F_h and f_h must be included in the B-L for them to be directly used as DV in the PDE editor.

The two last tasks needed to develop the numerical model are simpler than the previous tasks. First, a library with the physical parameters used in the equations must be created (PP-L, Task 6 in Fig. 3). It will include magnitudes like those in Table A2, which are related to the flow problem. Finally, the value of the material parameters relevant for each analysis must be defined and collected in a material parameters library (MP-L, Task 7, Fig. 3). Table 5 presents an example of the information to include.

5. Application examples. Basic code qualification

Following the guidelines suggested in the previous section, a THMc numerical solver has been developed using CM as the programming platform. This section presents three application examples. For each exercise, the initial and boundary conditions applied, and the material parameters used, are detailed. Therefore, in addition to illustrating the scope of the developed code, these exercises can be used by other researchers for a first qualification of their developed code.

5.1. Unsaturated infiltration test

This verification exercise analyzes the hydration of a cylindrical sample with a diameter of 20 cm and a height of 10 cm. The initial matric suction is 1 kPa ($P_L = 99$ kPa), there is no lateral flow, and the liquid pressure is set to zero at both the top and the bottom boundaries (see Fig. 4). A simplified conceptual model is adopted. The microstructural void ratio is assumed constant (disabling the PDE of the balance equation (2) in Table 2) and nearly zero. Therefore, a single porosity medium is analyzed. Balance equations (3)–(6) are also disabled (that is, constant gas pressure, set at the atmospheric pressure; constant salinity, set practically to zero; isothermal problem, with a constant temperature equal to 20 °C). In addition, the medium is treated as non-deformable, and the mechanical problem is not solved. Then, the total porosity, virtually equal to the macrostructural porosity, remains constant at a value of 0.32. Therefore, it is a problem where there is only water flow in a non-deformable medium. This illustrates the capacity of the numerical tool to be adapted to the constitutive model desired. In CM, disabling a PDE (and, in this case, also the two ODEs: the stress field and the preconsolidation stress are not updated since the medium is treated as non-deformable) only needs a click in the corresponding control box.

The example includes even more simplifications. Instead of using a retention curve based on van Genuchten [31] model, Sr_M is

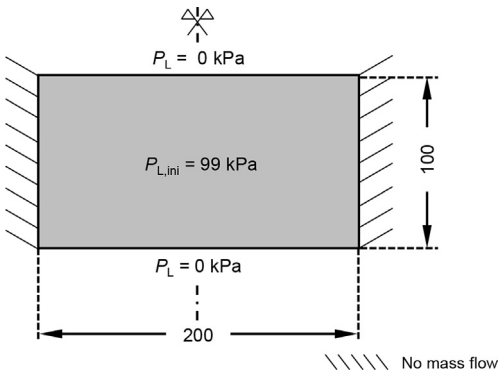

Fig. 4. Initial and boundary conditions of Exercise 5.1. Dimensions in mm.

Table 5
Material parameters used in Exercise 5.3. Parameter values from Navarro et al. [63].

	Magnitude	Definition	Value
Mechanical model	k	Slope of the increase in cohesion with suction	0.1
	κ_p	Saturated elastic stiffness for changes in p	0.1
	κ_S	Elastic stiffness for changes in s_M	0.05
	ν	Poisson's ratio	0.35
	p_C (kPa)	Reference stress of the net mean yield stress	10
	$\lambda(0)$	Saturated slope of the virgin compression curve	0.15
	r	Parameter of the macro-compressibility of the soil	0.8
	β (kPa^{-1})	Parameter of the macro-compressibility of the soil	2.0×10^{-5}
	M	Slope of the critical state line	1.07
Flow model	α (kPa^{-1})	van Genuchten parameter	1.15×10^{-4}
	m	van Genuchten parameter	0.733
	b_M	Intrinsic permeability parameter	9.911
	ϕ_{M0}	Intrinsic permeability parameter	0.047
	k_0 (m^2)	Intrinsic permeability parameter	2.339×10^{-21}

computed using the linear law # 1 from Table 6. In addition, the hydraulic conductivity will be assumed constant and equal to 3.1×10^{-12} m s^{-1}. These changes are attained by modifying the B-L.

As a result, this exercise shows the simplicity not only of scaling the complexity of the conceptual model but also of modifying the constitutive model by changing the state functions in the B-L. If it is of interest, the same can be done with the stress-strain model (see next section).

The simplifications introduced mean that the solved problem has an analytical solution. Fig. 5 compares the numerical solution with the analytical solution presented by Carslaw and Jaeger [64]. The fit is very satisfactory, constituting a first verification of the program developed.

5.2. Thermo-hydraulic cell test

This validation exercise simulates the thermohydraulic test # 8 performed by Villar et al. [65]. The material tested was a bentonite from Almeria (Spain) (95% montmorillonite; cation exchange capacity, *CEC*, 88 meq/100 g; exchangeable cations: Ca^{2+}, 42 meq/100 g; Mg^{2+}, 26 meq/100 g; Na^{+}, 18 meq/100 g; K^{+}, 2 meq/100 g; liquid limit, 213%; mineral density, 2.78 g/cm^3 [65]). A compacted sample (initial conditions: water content, 11.8%; dry density, 1.66 g/cm^3; temperature, 20 °C) was placed in a cylindrical stainless-steel cell with an internal diameter of 15.0 cm and an internal height of 14.6 cm. The cell had a 10.0 cm high central heater, resulting in a temperature gradient in both horizontal and vertical directions. The bentonite sample was wetted by its lower end. The test configuration and boundary conditions are shown in Fig. 6.

As in the previous exercise, the computation of the evolution of microstructure and salinity has been disabled in the numerical model. Water salinity and e_m are assumed constant and almost zero. In this case, the deformability of the macrostructure, the flow of water and air and heat transfer have been included in the analysis.

After the experimental work of Villar et al. [65], three modifications have been introduced in the B-L to show how easily the constitutive equations can be modified in the proposed numerical solver. First, the macrostructural degree of saturation for water is computed as indicated by equation # 2 in Table 6. Second, the intrinsic permeability for macrostructural liquid k_{ML} is defined by the exponential law identified as # 3 in Table 6. In addition, the relative permeability for macrostructural liquid κ_{ML} is computed with equation # 4 of Table 6. Last, instead of obtaining the thermal conductivity of the soil as a weighted average of all the species present, it was computed as $\lambda = 1.3\, Sr_M + 0.7\,(1 - Sr_M)$ W·m^{-1} K^{-1} (where 1.3 W m^{-1} K^{-1} is the thermal conductivity of saturated bentonite, and 0.7 W m^{-1} K^{-1} is that of dry bentonite). For the gas flow, the parameters $a_G = 4$ and $b_G = 10^{-12}$ are used (see Table A1).

The M-L has also been modified. A non-linear elastic behavior of the soil has been assumed, and the macrostructural void ratio e_M is defined with the logarithmic state surface identified as equation # 5 in Table 6, where p" is the net mean stress (defined as $p" = p - P_G$, where p is the total mean stress). Poisson's ratio is taken as 0.33, and the thermo-mechanical coupling is disregarded.

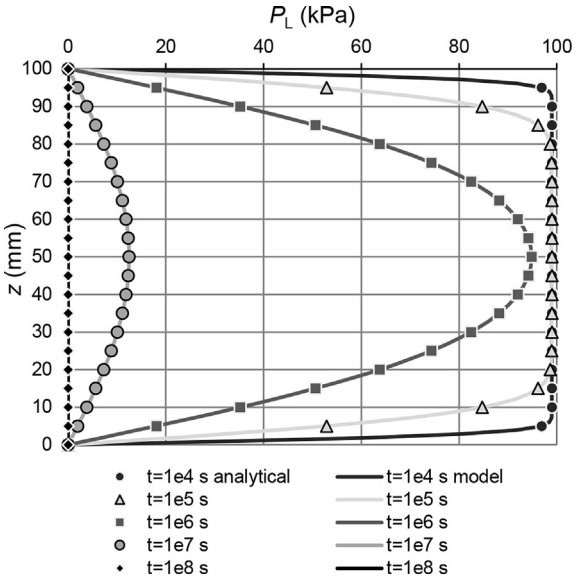

Fig. 5. Exercise 5.1. Temporal evolution of liquid pressure; analytical (markers) and numerical (lines) results.

Concerning the boundary conditions, the temperature of the heater (boundary C4 in Fig. 6) linearly increased from 20 °C to 96.5 °C along the first 30 min of the test. Afterward, this temperature remained constant until the end of the test (2401.6 h). At boundary C1 (Fig. 6), the water pressure increased to a constant value of 1100 kPa. For modeling purposes, this increase has been assumed to occur in the first minute of the test. According to Navarro and Alonso [29], the heat loss at boundaries C1, C2 and C3 has been computed as $q^* = -9\,(T - 293.15)$ W·m^{-2}, where T (K) is the temperature of the sample at the contact with the boundary. In addition, displacements normal to the boundaries were prevented in all of them.

Given the test configuration, the analysis performed is axisymmetric. Fig. 7a compares experimental and numerical results for the water intake along the test. The fit obtained is very satisfactory, as well as the results for Sr_M at the end of the test, Fig. 8a.

The fit of T in Fig. 8b also represents its spatial distribution. In this case, the results are represented at 25.6 h from the beginning of the test, to show that the spatial distribution of the system behavior is reproduced not only at the end but also along the test. This is clearer in Fig. 7b, which plots the time evolution of temperature at the thermocouples installed in the sample (see Fig. 6).

5.3. Simulation of a vertical free swelling test

The quality of the results obtained in the two previous exercises contribute to the confidence in the capacity of the model to reproduce the THM behavior of compacted bentonites. However, those tests did not include the effect of salinity. This new validation

Table 6
Constitutive simplifications introduced in Examples 5.1 and 5.2

Equation #	Law	Section
1	$Sr_M = 1 - 4.13 \times 10^{-3} s_M$, s_M in kPa	5.1
2	$Sr_M = 0.95 - 0.596 \tanh(9.4 \times 10^{-6} s_M)$, s_M in kPa	5.2
3	$k_{ML} = 0.97931 \times 10^{-24} \times 10^{5\, e_M}$, k_{ML} in m^2	5.2
4	$\kappa_{ML} = \left(\frac{Sr_M - 0.05}{0.95}\right)^3$	5.2
5	$e_M = 1.64047 - 0.31 \log_{10}(p") - 0.155 \log_{10}(s_M) + 0.048 \log_{10}(p") \log_{10}(s_M)$, $p"$ and s_M in kPa	5.2

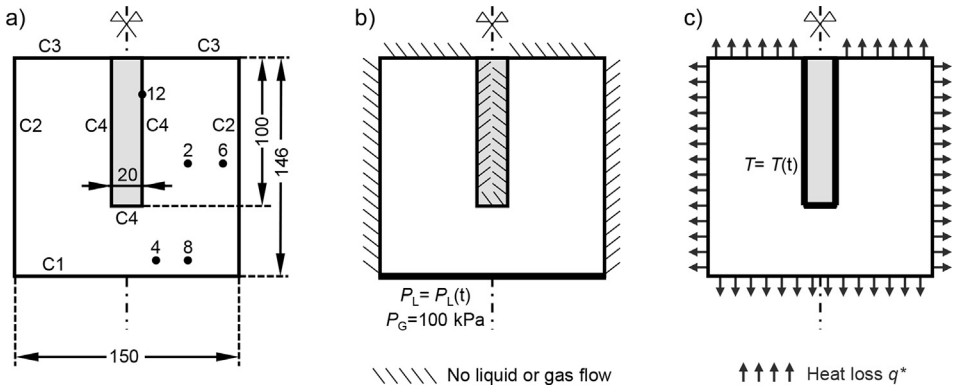

Fig. 6. Exercise 5.2: (a) test configuration (dimensions in mm) and position of thermocouples (points); (b) hydraulic boundary conditions; (c) thermal boundary conditions.

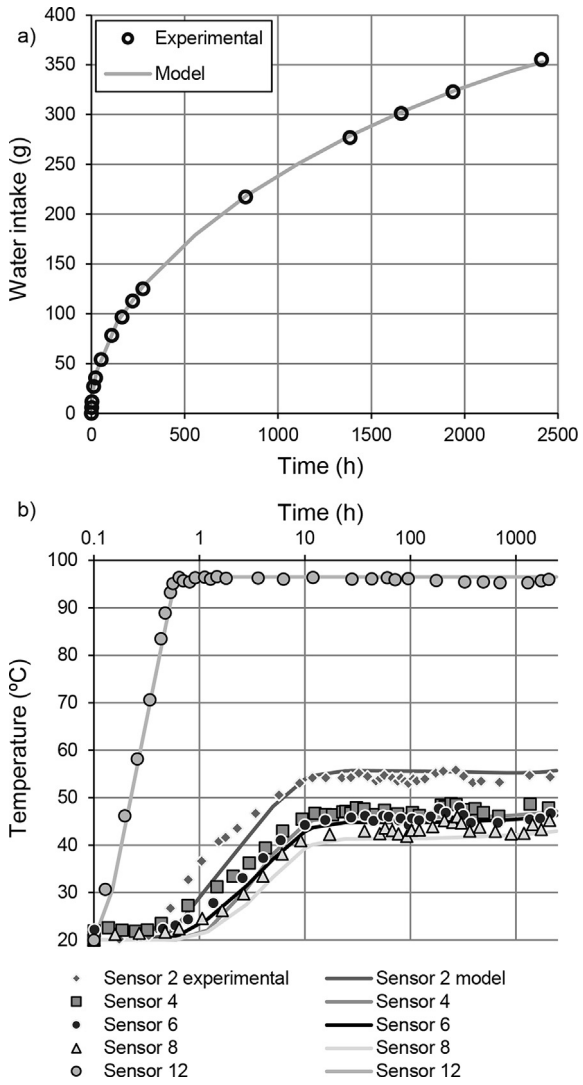

Fig. 7. Exercise 5.2: (a) Water intake evolution with time. (b) Temperature evolution (experimental, markers, and numerical, lines) with time in the thermocouples defined in Fig. 6.

exercise does, which analyzes free swelling, one of the processes with a strongest chemo-mechanical coupling in bentonites.

The vertical free swelling tests presented by Navarro et al. [10] are simulated. The experiments tested a Wyoming MX-80 bentonite (87.6% smectite; *CEC*, 84 meq/100 g; exchangeable cations: Ca^{2+}, 25 meq/100 g; Mg^{2+}, 8 meq/100 g; Na^{+}, 58 meq/100 g; K^{+}, 2 meq/100 g; liquid limit, 510%; mineral density, 2.78 g/cm^3 [66]). Cylindrical samples were prepared with deionized water and compacted to a height of 4 cm and a diameter of 5 cm, with an initial bulk density of 2.05 g/cm^3 and a water content of a 17%. Subsequently, the samples were tightly fitted at the bottom of a transparent tube. Thus, the swelling caused after adding an aqueous solution of a determined concentration over the samples was only vertical. The analysis focuses on the hydration with three solutions: deionized water, a 10 g/L solution (6.47 g/L of NaCl and 3.53 g/L of $CaCl_2$), and a 35 g/L solution (16.75 g/L of NaCl and 18.25 g/L of $CaCl_2$). Fig. 9 outlines the test layout and the boundary conditions applied in the simulation. As noted at the end of Section 3, a Lagrangian formulation is used to model the finite strains associated with swelling. The geochemical model assumed in this work is deemed as a valid conceptual frame to reproduce the tests, since the analyzed bentonite is mainly sodic, and the hydrating solutions only include calcium, sodium and chloride. Therefore, the solution of the balance of calcium and chloride characterizes the evolution of salinity along the test. To simulate the swelling caused by the destructuration of microstructure, e_m needs to be solved. In addition, the kinetics of the process is directly linked to the hydration of the sample, and consequently the macrostructural water mass balance is also solved. On the other hand, the air mass balance has been disabled, and the gas pressure is set to the atmospheric pressure. The enthalpy balance has also been disabled, and isothermal conditions are assumed (T equals 20 °C). The mechanical problem is solved (the medium is deformable), and the time integration of net stresses and preconsolidation stress is solved. Table 5 includes the parameters used for the mechanical, flow and transport models.

Fig. 10 compares the free swelling obtained with the model and the experimental measurements. The fit is very satisfactory. However, like water intake in the exercise in Section 5.2, swelling is an integrated magnitude, providing only one value at each time for the whole sample. In this case, space distributed values are not available for different times. Only the final (post-mortem) values of water content w and dry density ρ_D, measured following conventional procedures (following standards ASTM D2216-10 [67], for w, and ASTM D7263-09(2018)e1 [68], for ρ_D), are available. Nevertheless, and even if the softness of the soil made it impossible to take samples to determine ρ_D at the top of the sample, the fits represented in Figs. 11 and 12 are also satisfactory. Although the conceptual model for free swelling is still under development, the framework of MPDES allows to implement the existing models, with encouraging results, and contributes to the development of new models by making their numerical implementation easier.

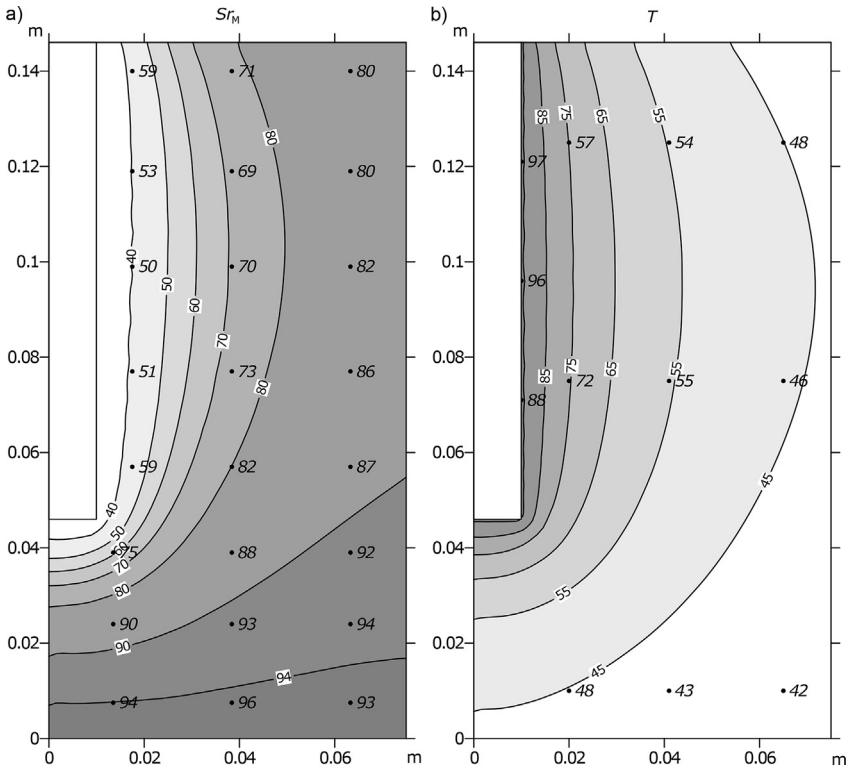

Fig. 8. Exercise 5.2: comparison of experimental (numbered points) and numerical (contours) results. (a) Final distribution of the degree of saturation. (b) Temperature distribution after 25.6 h.

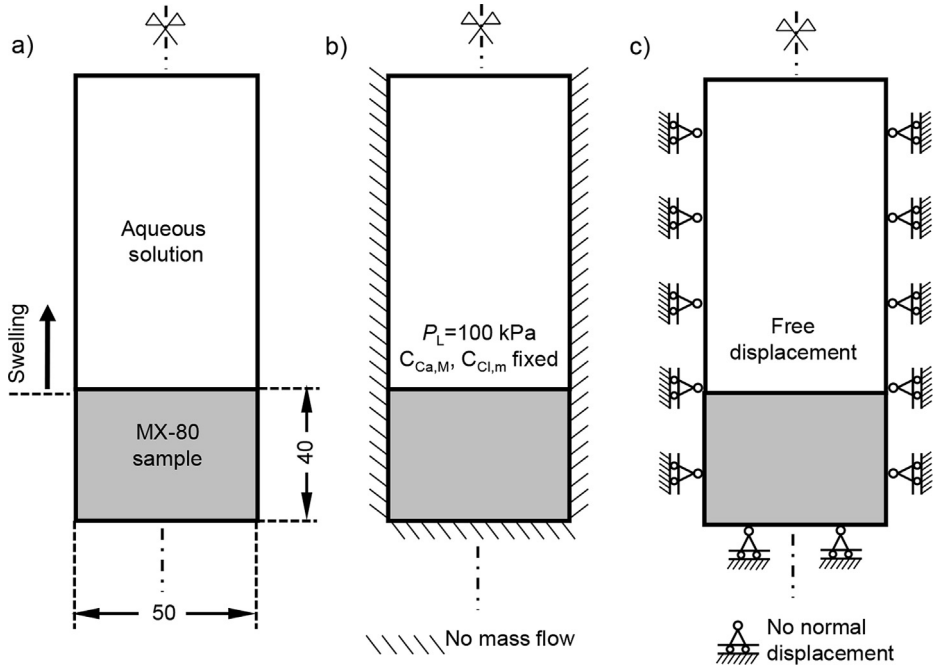

Fig. 9. Exercise 5.3: (a) test configuration, and (b) flow and transport and (c) mechanical boundary conditions considered in the simulation. Dimensions in mm.

6. Conclusions

This paper presents a conceptual model based on the review and selection of the reference formulations used to simulate the thermo-hydro-chemo-mechanical behavior of compacted bentonites. The model is able to characterize the main features of the behavior of the clay-based engineered barriers considered for deep geological repositories of high level radioactive waste. However, to estimate the behavior of these barriers reasonably, numerical tools are necessary that, after having implemented the mentioned models, are capable to simulate the response of the system under different conditions and analysis.

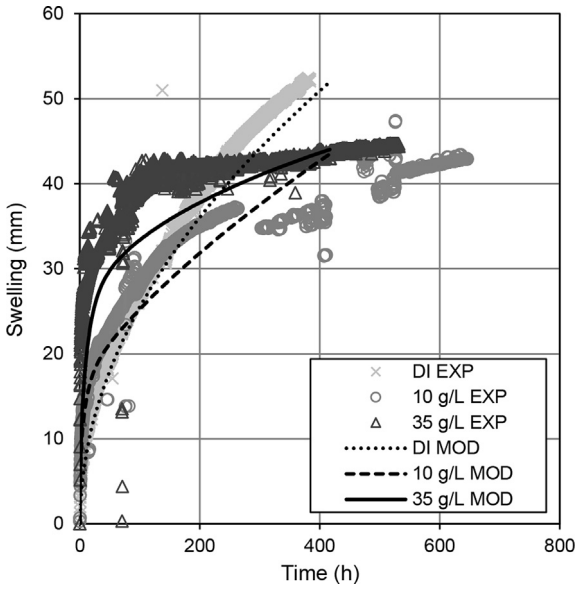

Fig. 10. Experimental (markers) and numerical (lines) results of the free swelling tests in Exercise 5.3., when hydrating bentonite with deionized water, 10 g/L concentration solution and 35 g/L concentration solution.

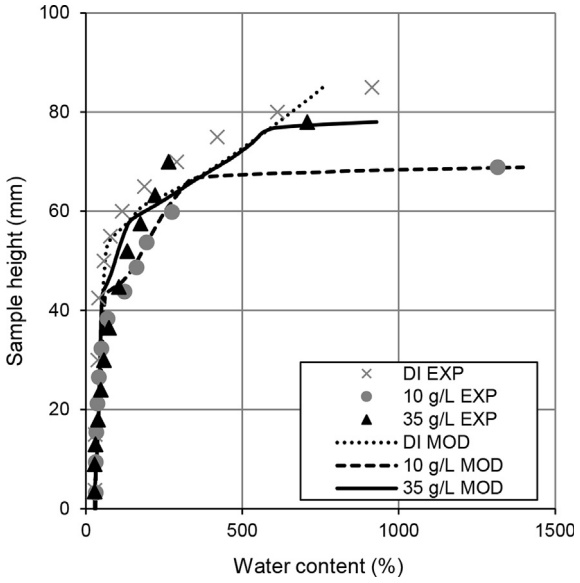

Fig. 11. Experimental (markers) and numerical (lines) results for the water content distribution at the end of the tests in Exercise 5.3., when hydrating bentonite with deionized water, 10 g/L concentration solution and 35 g/L concentration solution.

The guidelines proposed in Section 4 (Fig. 3) outline the development of such tools that use multiphysical partial differential equations solvers as implementation platforms. This is illustrated by the code developed, which obtained the results presented in Figs. 5 and 7 and 8 and 10–12. The multiphysics environment enables an easy scaling of the tool, to adapt it to the conceptual model desired for each problem. This way, the same tool can be used to approach the same problem at different complexity levels. The simulations performed, especially that in Section 5.1, are an example of this scaling capacity. Without overlooking the difficulty of these solvers to implement complex geochemical models and to simulate localization processes, new physical processes and

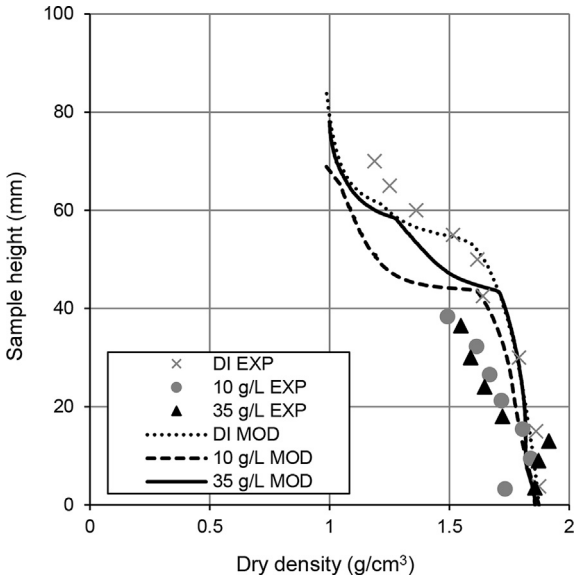

Fig. 12. Experimental (markers) and numerical (lines) results for the dry density distribution at the end of the tests in Exercise 5.3., when hydrating bentonite with deionized water, 10 g/L concentration solution and 35 g/L concentration solution.

constitutive models can be introduced in the future to improve the conceptual model adopted.

Besides, thanks to automatic symbolic differentiation, the system iteration matrix is of high quality, which improves the numerical performance of the solver. In addition, symbolic algebra offers a friendly programming environment, as the code implementation is based on writing functions in a text format, constituting "libraries" that can be read from a text file (Section 4). Then, to change a constitutive model or a state function, it is enough to edit the corresponding library and write a new function with the text processor. This was done in the exercises in Sections 5.1 and 5.2.

This shows that multiphysics partial differential equations solvers able to perform symbolic computations, such as Comsol Multiphysics, are a tool of value to research groups interested in having a code to simulate the behavior of clay-based engineered barriers. For these groups, while it is always advisable to complement the verification and validation effort, the three application exercises presented are a notable qualification approach, providing a good starting point for building confidence in the models developed.

Acknowledgments

This study was funded by Posiva Oy projects 2108211 and 2113799, and by FPU Grant FPU15/02655 from the Spanish Ministry of Education awarded to Ms. De la Morena.

Appendix A. Flow problem

Table A1 contains the dependent variables that control the flow problem, which are involved in the state functions in Table 3 and the field equations in Table 4. In the last column, if applicable, the references that describe the proposed formulation are included. Table A2 contains the physical parameters used in the flow model.

Table A1
Dependent variables of the flow problem

Magnitude	Expression	Refs
a_M	$1 - 0.017 \sum c_{iM}$	[69,70]
c_{iM}	$\frac{C_{iM}}{\rho_W}$	
D_V	$5.9 \times 10^{-6} \frac{T^{2.3}}{P_G}$	[30]
H	$7.121183 \times 10^{-11}\ T\ \rho_W \exp\left(\frac{1997.392}{T}\right)$	[42]
k_{ML}	$k_O \exp(b_M(\varphi_M - \varphi_{MO}))$	[7]
k_G	$b_G(e_M)^{a_G}$	[34]
n	$\frac{1}{1-m}$	[31]
P_A	$P_G - P_V$	
P_V	$\frac{\rho_V R\, T}{WMM}$	
s_{MTOT}	$s_M + s_{MO}$	
s_{MO}	$-\frac{\rho_W}{WMM} R\, T\, Ln\,(a_M)$	
Sr_M	$\frac{1}{(1+(\alpha\, s_M)^n)^m}$	[31]
κ_{ML}	Sr_M^3	[7]
κ_G	$(1 - Sr_M)^{a_G}$	[34]
ϕ_M	$\frac{e_M}{1+e}$	
ρ_A	$\frac{AMM\ P_A}{R\ T}$	
ρ_G	$\rho_A + \rho_V$	
ρ_V	$\rho_{VO}\ \exp\left(-\frac{WMM}{\rho_W R\ T} s_{MTOT}\right)$	[40]
ρ_{VO}	$\frac{\exp(0.06374\ (T+273.15) - 0.1634 \times 10^{-3}\ (T+273.15)^2)}{194.4}$	[41]

Table A2
Physical parameters

Magnitude	Definition	Value
AMM	Molar mass of air	28.97 g mol^{-1}
g	Gravitational acceleration	9.81 m s^{-2}
R	Universal gas constant	8.31 J K^{-1} mol^{-1}
WMM	Molar mass of water	18.02 g mol^{-1}
ρ_W	Density of free liquid water	1000 kg m^{-3}

References

[1] European Commission, Geological Disposal of Radioactive Wastes Produced by Nuclear Power: from Concept to Implementation, European Commission, Luxembourg, 2004.
[2] OECD-NEA, Engineered Barrier Systems and the Safety of Deep Geological Repositories, State-Of-The-Art Report, OECD-NEA, Paris, 2003.
[3] R. Pusch, The performance of clay barriers in repositories for high-level radioactive waste, Nucl. Eng. Technol. 38 (6) (2006) 483–488.
[4] P. Sellin, O.X. Leupin, The use of clay as an engineered barrier in radioactive-waste management - a review, Clay Clay Miner. 61 (6) (2013) 477–498.
[5] Posiva, Safety Case for the Disposal of Spent Nuclear Fuel at Olkiluoto - Synthesis 2012, Posiva 2012-12, Posiva Oy, 2012, www.posiva.fi/files/2987/Posiva_2012-12web.pdf. accessed: January 2019.
[6] O. Karnland, A. Muurinen, F. Karlsson, Bentonite swelling pressure in NaCl solutions - experimentally determined data and model calculations, in: E.E. Alonso, A. Ledesma (Eds.), Advances in Understanding Engineered Clay Barriers: Proceedings of the International Symposium on Large Scale Field Tests in Granite, Sitges, Barcelona, 12-14 November 2003, Taylor and Francis Group, London, 2005, pp. 241–256.
[7] A. Gens, B. Valleján, M. Sánchez, C. Imbert, M.V. Villar, M. van Geet, Hydro-mechanical behaviour of a heterogeneous compacted soil: experimental observations and modelling, Geotechnique 61 (5) (2011) 367–386.
[8] M. Sánchez, A. Gens, M.V. Villar, S. Olivella, Fully coupled thermo-hydro-mechanical double-porosity formulation for unsaturated soils, Int. J. Geomech. 16 (6) (2016).
[9] L.D.N. Guimarães, A. Gens, M. Sánchez, S. Olivella, A chemo-mechanical constitutive model accounting for cation exchange in expansive clays, Geotechnique 63 (3) (2013) 221–234.
[10] V. Navarro, Á. Yustres, L. Asensio, G. De la Morena, J. González-Arteaga, T. Laurila, X. Pintado, Modelling of compacted bentonite swelling accounting for salinity effects, Eng. Geol. 223 (2017) 48–58.
[11] COMSOL, COMSOL Multiphysics Reference Manual, 2015 version 5.12015.
[12] J.R.R.A. Martins, J.T. Hwang, Review and unification of methods for computing derivatives of multidisciplinary computational model, AIAA J. 51 (11) (2013) 2582–2599.
[13] E. Romero, A. Gens, A. Lloret, Water permeability, water retention and microstructure of unsaturated compacted Boom clay, Eng. Geol. 54 (1–2) (1999) 117–127.
[14] A. Gens, E.E. Alonso, A framework for the behaviour of unsaturated expansive clays, Can. Geotech. J. 29 (6) (1992) 1013–1032.
[15] R.N. Yong, Overview of modeling of clay microstructure and interactions for prediction of waste isolation barrier performance, Eng. Geol. 54 (1–2) (1999) 83–91.
[16] T.A. Hueckel, Water-mineral interaction in hygromechanics of clays exposed to environmental loads: a mixture-theory approach, Can. Geotech. J. 29 (6) (1992) 1071–1086.
[17] V. Navarro, E.E. Alonso, Secondary compression of clays as a local dehydration process, Geotechnique 51 (10) (2001) 859–869.
[18] V. Navarro, L. Asensio, G. De la Morena, X. Pintado, Á. Yustres, Differentiated intra-and inter-aggregate water content models of mx-80 bentonite, Appl. Clay Sci. 118 (2015) 325–336.
[19] A.C. Jacinto, M.V. Villar, A. Ledesma, Influence of water density on the water-retention curve of expansive clays, Geotechnique 62 (8) (2012) 657–667.
[20] C. Tournassat, C.A.J. Appelo, Modelling approaches for anion-exclusion in compacted Na-bentonite, Geochem. Cosmochim. Acta 75 (13) (2011) 3698–3710.
[21] P.G. Studds, D.I. Stewart, T.W. Cousens, The effects of salt solutions on the properties of bentonite-sand mixtures, Clay Miner. 33 (4) (1998) 651–660.
[22] Á. Yustres, A. Jenni, L. Asensio, X. Pintado, K. Koskinen, V. Navarro, P. Wersin, Comparison of the hydrogeochemical and mechanical behaviours of compacted bentonite using different conceptual approaches, Appl. Clay Sci. 141 (2017) 280–291.
[23] V. Navarro, G. De la Morena, Á. Yustres, J. González-Arteaga, L. Asensio, Predicting the swelling pressure of MX-80 bentonite, Appl. Clay Sci. 149 (2017) 51–58.
[24] F. Helfferich, Ion Exchange. Series in Advanced Chemistry, McGraw-Hill, New York, 1962.
[25] Posiva, Safety Case for the Disposal of Spent Nuclear Fuel at Olkiluoto - Features, Events and Processes 2012, Posiva 2012-07, Posiva Oy, 2012, www.posiva.fi/files/2994/Posiva_2012-07.pdf. accessed: January 2019.
[26] S. Olivella, E.E. Alonso, Gas flow through clay barriers, Geotechnique 58 (3) (2008) 157–176.
[27] D.G. Fredlund, H. Rahardjo, M.D. Fredlund, Unsaturated Soil Mechanics in Engineering Practice, John Wiley and Sons, Hoboken, New Jersey, 2012.
[28] K. Ikonen, J. Kuutti, H. Raiko, Thermal Dimensioning for the Olkiluoto Repository – 2018 Update, Posiva Working Report 2018-26, Posiva Oy, 2018, www.posiva.fi/files/4973/WR_2018-26_web.pdf. accessed: January, 2019.
[29] V. Navarro, E.E. Alonso, Modeling swelling soils for disposal barriers, Comput. Geotech. 27 (1) (2000) 19–43.

[30] D.W. Pollock, Simulation of fluid flow and energy transport processes associated with high-level radioactive waste disposal in unsaturated alluvium, Water Resour. Res. 22 (5) (1986) 765–775.
[31] M.T. van Genuchten, A closed-form equation for predicting the hydraulic conductivity of unsaturated soils, Soil Sci. Soc. Am. J. 44 (5) (1980) 892–898.
[32] R.M. Brooks, A.T. Corey, Hydraulic Properties of Porous Media, Colorado State University, Fort Collins, Colorado, 1964.
[33] B.R. Scanlon, J.P. Nicot, J.W. Massmann, Soil gas movement in unsaturated systems, in: A.W. Warrick (Ed.), Soil Physics Companion, Taylor and Francis Group, Boca Raton, Florida, 2002, pp. 297–341.
[34] Y. Yoshimi, J.O. Ostenberg, Compression of partially saturated cohesive soils, J. Soil Mech. Found Div. 89 (4) (1963) 1–24.
[35] M.V. Villar, A. Lloret, Variation of the intrinsic permeability of expansive clay upon saturation, in: K. Adachi, M. Fukue (Eds.), Clay Science for Engineering, Balkema, Rotterdam, 2001, pp. 259–266.
[36] S.M. Hassanizadeh, Derivation of basic equations of mass transport in porous media, Part 2. Generalized Darcy's and Fick's laws, Adv. Water Resour. 9 (4) (1986) 207–222.
[37] J.R. Philip, D.A. De Vries, Moisture movement in porous materials under temperature gradients, Eos Trans. Am. Geophys. Union 38 (2) (1957) 222–232.
[38] S. Olivella, A. Gens, Vapour transport in low permeability unsaturated soils with capillary effects, Transport Porous Media 40 (2) (2000) 219–241.
[39] X. Pintado, A. Ledesma, A. Lloret, Backanalysis of thermohydraulic bentonite properties from laboratory tests, Eng. Geol. 64 (2002) 91–115.
[40] N.E. Edlefsen, A.B.C. Anderson, Thermodynamics of soil moisture, Hilgardia 15 (2) (1943) 31–298.
[41] J. Ewen, H.R. Thomas, Heating unsaturated medium sand, Geotechnique 39 (3) (1989) 455–470.
[42] D.G. Fredlund, H. Rahardjo, Soil Mechanics for Unsaturated Soils, John Wiley and Sons, New York, 1993.
[43] J. Šimunek, M.T. van Genuchten, Contaminant transport in the unsaturated zone. Theory and modelling, in: J.W. Delleur (Ed.), The Handbook of Groundwater Engineering, second ed., CRC Press, 2006, 22.1-2.46.
[44] I.C. Bourg, G. Sposito, A.C.M. Bourg, Tracer diffusion in compacted, water-saturated bentonite, Clay Clay Miner. 54 (3) (2006) 363–374.
[45] E.L. Cussler, Diffusion: Mass Transfer in Fluid Systems, second ed., Cambridge University Press, 1997.
[46] A. Lloret, M.V. Villar, Advances on the knowledge of the thermo-hydro-mechanical behaviour of heavily compacted "FEBEX" bentonite, Phys. Chem. Earth 32 (8–14) (2007) 701–715.
[47] E.E. Alonso, A. Gens, A. Josa, A constitutive model for partially saturated soils, Geotechnique 40 (3) (1990) 405–530.
[48] D. Sheng, S.W. Sloan, A. Gens, A constitutive model for unsaturated soils: thermomechanical and computational aspects, Comput. Mech. 33 (6) (2004) 453–465.
[49] D. Sheng, Review of fundamental principles in modelling unsaturated soil behaviour, Comput. Geotech. 38 (6) (2011) 757–776.
[50] C. Ma, T. Hueckel, Stress and pore pressure in saturated clay subjected to heat from radioactive waste: a numerical simulation, Can. Geotech. J. 29 (6) (1992) 1087–1094.
[51] V. Navarro, G. De la Morena, J. González-Arteaga, Á. Yustres, L. Asensio, A microstructural effective stress definition for compacted active clays, Geomech. Energy Env. 15 (2018) 47–53.
[52] A. Dueck, U. Nilsson, Thermo-Hydro-Mechanical Properties of MX-80. Results from Advanced Laboratory Tests. SKB Technical Report TR-10-55, Svensk Kärnbränslehantering AB, Swedish Nuclear Fuel and Waste Management Co, 2010. January 2019, www.skb.com/publication/2223073/TR-10-55.pdf.
[53] G. Kahr, F. Kraehenbuehl, H.F. Stoeckli, M. Muller-Vonmoos, Study of the water-bentonite system by vapour adsorption, immersion calorimetry and X-ray techniques. II. Heats of immersion, swelling pressures and thermodynamic properties, Clay Miner. 25 (4) (1990) 499–506.
[54] P. Sane, T. Laurila, M. Olin, K. Koskinen, Current Status of Mechanical Erosion Studies of Bentonite Buffer, Posiva Report 2012-45, Posiva Oy, 2013, www.posiva.fi/files/3349/POSIVA_2012-45.pdf. accessed: January 2019.
[55] L. Wadsö, K. Svennberg, A. Dueck, An experimentally simple method for measuring sorption isotherms, Dry. Technol. 22 (10) (2004) 2427–2440.
[56] E.E. Alonso, J. Vaunat, A. Gens, Modelling the mechanical behaviour of expansive clays, Eng. Geol. 54 (1–2) (1999) 173–183.
[57] F. Salles, J.M. Douillard, R. Denoyel, O. Bildstein, M. Jullien, I. Beurroies, H. Van Damme, Hydration sequence of swelling clays: evolutions of specific surface area and hydration energy, J. Colloid Interface Sci. 333 (2) (2009) 510–522.
[58] M.K. Gobbert, A. Churchill, G. Wang, T.I. Seidman, COMSOL Multiphysics for efficient solution of a transient reaction-diffusion system with fast reaction, in: Y. Rao (Ed.), Proceedings of the COMSOL Conference, Boston, 2009.
[59] V. Navarro, L. Asensio, J. Alonso, Á. Yustres, X. Pintado, Multiphysics implementation of advanced soil mechanics models, Comput. Geotech. 60 (2014) 20–28.
[60] J. Alonso, V. Navarro, B. Calvo, L. Asensio, Hydro-mechanical analysis of CO2 storage in porous rocks using a critical state model, Int. J. Rock Mech. Min. Sci. 54 (2012) 19–26.
[61] M. Cervera, M. Chiumenti, R. Codina, Mixed stabilized finite element methods in nonlinear solid mechanics. Part I: formulation, Comput, Meth. Appl. Mech. Eng. 199 (37–40) (2010) 2559–2570.
[62] V. Navarro, L. Asensio, Á. Yustres, G. De la Morena, X. Pintado, Swelling and mechanical erosion of MX-80 bentonite: pinhole test simulation, Eng. Geol. 202 (2016) 99–113.
[63] V. Navarro, G. De la Morena, Á. Yustres, R. López-Vizcaíno, L. Asensio, A Numerical Inspection on the Squeezing Test in Active Clays, Géotechnique, 2018, https://doi.org/10.1680/jgeot.17.P.187. Ahead of Print.
[64] H.S. Carslaw, J.C. Jaeger, Conduction of Heat in Solids, second ed., Claredon Press, Oxford, 1959.
[65] M.V. Villar, J. Cuevas, P.L. Martin, R. Campos, A.M. Fernández, Thermo-Hydro-Mechanical Characterization of the Spanish Reference Clay Material for Engineered Barrier for Granite and Clay HLW Repository: Laboratory and Small Mock-Up Testing, Publicación Técnica 03/95, ENRESA, 1995. January 2019, www.iaea.org/inis/collection/NCLCollectionStore/_Public/26/067/26067405.pdf.
[66] L. Kiviranta, S. Kumpulainen, Quality Control and Characterization of Bentonite Materials, Posiva Working Report 2011-84, Posiva Oy, 2011. January 2019, www.posiva.fi/files/1994/WR_2011-84_web.pdf.
[67] ASTM D2216-10, Standard Test Methods for Laboratory Determination of Water (Moisture) Content of Soil and Rock by Mass, ASTM International, West Conshohocken, PA, 2010.
[68] ASTM D7263-09(2018)e1, Standard Test Methods for Laboratory Determination of Density (Unit Weight) of Soil Specimens, ASTM International, West Conshohocken, PA, 2018.
[69] R.M. Garrels, C.H. Christ, Solutions, Minerals, and Equilibria, Harper and Row, New York, 1965.
[70] D.L. Parkhurst, C.A.J. Appelo, Description of input and examples for PHREEQC version 3 - a computer program for speciation, batch-reaction, one-dimensional transport, and inverse geochemical calculations, U.S. Geol. Surv. Tech. Meth. (2013) 497, book 6, chap. A43.